Simultaneous spatial, conformational, and mass analysis of intact proteins and protein assemblies by nano-DESI travelling wave ion mobility mass spectrometry imaging

Hale, Oliver; Hughes, James; Cooper, Helen

DOI:
10.1016/j.ijms.2021.116656

Document Version
Peer reviewed version

Citation for published version (Harvard):
Hale, O, Hughes, J & Cooper, H 2021, 'Simultaneous spatial, conformational, and mass analysis of intact proteins and protein assemblies by nano-DESI travelling wave ion mobility mass spectrometry imaging', *International Journal of Mass Spectrometry*, vol. 468, 116656. https://doi.org/10.1016/j.ijms.2021.116656

Simultaneous spatial, conformational, and mass analysis of intact proteins and protein assemblies by nano-DESI travelling wave ion mobility mass spectrometry imaging.

Oliver J. Hale, James W. Hughes and Helen J. Cooper*

School of Biosciences, University of Birmingham, Edgbaston B15 2TT, U.K.

*To whom correspondence should be addressed: h.j.cooper@bham.ac.uk

Abstract

We have previously demonstrated native nano-desorption electrospray ionization (nano-DESI) mass spectrometry imaging of proteins and protein complexes in thin tissue section of rat kidney. Here, we demonstrate the integration of travelling wave ion mobility spectrometry (TWIMS) into the native nano-DESI MSI workflow. The benefits of TWIMS are twofold: Firstly, arrival time filtering allows subtraction of chemical noise and the resulting ion images show improved specificity. Secondly, the incorporation of TWIMS enables the calculation of collision cross sections, and thus a measure of protein structure, directly from the imaging dataset. Our results show good agreement between the collision cross sections determined from nano-DESI, which requires the use of a heated inlet, and those determined experimentally from liquid extraction surface analysis (LESA) with an ambient temperature inlet, and those available in the literature. Ion images and collision cross sections are presented for a range of proteins and protein assemblies with molecular weights of up to 42.6 kDa.

Introduction

We have recently demonstrated the application of nanospray-desorption electrospray ionization (nano-DESI) to native mass spectrometry imaging (MSI) of proteins in thin tissue sections.[1] Native nano-DESI MSI incorporates the benefits of native mass spectrometry and ambient mass spectrometry, and offers higher spatial resolution than liquid extraction surface analysis (LESA) MSI, the only other technique so far applied to the native MSI of proteins from tissue.[2-4]

Native mass spectrometry (MS) refers to electrospray ionization of proteins from solutions designed to mimic physiological conditions and is characterized by the retention of solution-phase non-covalent interactions in the gas phase. Native MS enables the mass and stoichiometry of intact protein assemblies to be determined,[5] and can include ion mobility spectrometry (IMS) performed in tandem on the same instrumentation. Integration of IMS can provide structural information in the form of the rotationally averaged collision cross section (CCS).[6-8] Since the CCSs of intact proteins are related to their three-dimensional structure, the degree to which a protein is folded can be assessed from the CCS values. Incorrectly folded proteins can adopt detrimental function, or be unable to provide a critical function, and are implicated in diseases such as Alzheimer's disease, prion diseases and kidney diseases.[9,10,11] Typically, native MS studies are performed on recombinant protein samples; however, the ability to analyze intact proteins from animal and human samples *in situ* could further our understanding of disease progression and guide the development of treatments and therapies.

In situ mass spectrometry has been a highly active research area for the last two decades, with ambient mass spectrometry techniques such as desorption electrospray ionization (DESI)[12], liquid extraction surface analysis (LESA)[13], and nanospray-desorption electrospray ionization (nano-DESI)[14] being introduced. The distribution of molecules within a sample can be mapped under ambient conditions by harnessing these techniques for MSI. Denatured protein MSI from tissue, with a spatial resolution >150 μm, has been performed using DESI coupled to ion mobility separation.[15,16] Nano-DESI has been demonstrated at spatial resolutions of around 10 μm for small molecules[17,18], and approx. 200 μm for denatured and folded proteins.[1,19,20] Spatially-targeted proteomic analysis by LESA-like techniques has been performed in a bottom-up fashion using both microLESA[24] and the nanoPOTS workflow[25], featuring sampling diameters of approx. 100 μm, whereas native LESA of intact proteins has been limited to a pixel size of approx. 1 mm.[2-4] Other ambient ionization techniques have yet to address intact protein MSI but are potential candidates for development. For example, tapping-mode scanning probe electrospray ionization (t-SPESI) has achieved spatial resolution of approx. 6 μm and laser desorption/ionization droplet delivery (LDIDD) has achieved up

to ~3 μm for imaging of small molecules.[26,27] *In situ* native mass spectrometry remains challenging because of factors including ion suppression and low analyte concentration limiting the numbers of proteins that can be detected. Nevertheless, we have demonstrated LESA and nano-DESI MSI of folded proteins and protein complexes in tissue[1-3] and Sharon and coworkers have analyzed protein complexes from crude cell lysates.[28]

Building on earlier work[15,29-31] which demonstrated the benefits of ion mobility spectrometry for MSI of intact, but unfolded proteins, we previously integrated travelling wave ion mobility spectrometry (TWIMS[32]) with native LESA MSI[2,4] and high field asymmetric waveform ion mobility spectrometry (FAIMS[33]) with *in situ* native MS.[34] Native LESA TWIMS MSI provided simultaneous spatial, conformational and mass information for intact protein complexes in a single MSI experiment.[4] In this study, we have integrated native nano-DESI MSI with TWIMS. Nano-DESI has previously been coupled to drift tube ion mobility-mass spectrometry for the analysis of lipids to produce ion images for ions of specific drift times, although without determining lipid CCS.[35] Our aim was to exploit the capability for TWIMS arrival time (t_A) filtering to produce ion images with improved specificity and to reveal new or overlapping molecule distributions, and determine the CCSs of endogenous proteins and protein assemblies from the imaging data. Initially, we considered the effect of the heated inlet, necessary for desolvation of ions in native nano-DESI, on the calculated CCS values of previously identified and spatially mapped[1,3] proteins from rat kidney to understand whether unfolding occurred during analysis. $^{TW}CCS_{N2\rightarrow He}$, i.e., CCSs obtained using a travelling wave device where the bath gas was N_2, and calibrated with CCS from drift tube ion mobility measurements in He,[7] were compared to those obtained by native LESA and values found in the literature. $^{TW}CCS_{N2\rightarrow He}$ were similar between nano-DESI and LESA experiments indicating no unfolding. We demonstrate the use of TWIMS-MSI to increase the specificity of ion signals in nano-DESI images, and show ion images of intact proteins and protein assemblies with molecular weight up to 42.6 kDa.

Materials and Methods

MS-grade water, methanol and formic acid were purchased from Fisher Scientific (Loughborough, UK). HPLC-grade ammonium acetate was bought from J.T. Baker (Deventer, Netherlands). C_8E_4 detergent and the protein standards ubiquitin (bovine, U6253), cytochrome C (equine, C2506) and myoglobin (equine, M0630) were obtained from Sigma-Aldrich (Gillingham, UK). The solvent system used for producing ion images was ammonium acetate (200 mM) + 0.125% C_8E_4 detergent. Sodium iodide (2 μg/μL in 50% isopropanol) for TOF mass calibration was obtained from Waters Corporation

(Manchester, UK). Argon (purity > 99.998%), nitrogen (>99.995%) and helium (>99.996%) gases were obtained from BOC (Guildford, UK).

Animal Tissue

Kidney tissue from a vehicle-dosed (0.5% HPMC & 0.1% tween 80 in water) adult male Hans Wistar rat was the kind gift of Dr Richard Goodwin (Astra Zeneca). The animal was euthanized two hours post dose. Dissection was performed by trained AstraZeneca staff (project licence PP77366793, procedure number 3). Kidneys were snap-frozen in isopropanol over dry ice. All tissue was stored at -80 °C and sectioned at -22 °C to a thickness of 10 μm with a CM1810 Cryostat (Leica Microsystems, Wetzlar, Germany) and thaw mounted to glass microscope slides. Sections were stored at -80 °C until use. Tissue sections were not subjected to any washing protocol prior to analysis. Bright field microscopy was performed post-MSI to create digital images of the entire section. This was performed using an Axio Scan.Z1 (Carl Zeiss AG, Oberkochen, Germany) with 10x magnification and Image analysis was performed using Zeiss Zen lite.

Nano-DESI ion source

A 2D DESI ion source (Prosolia Inc., Indiana, Indianapolis) was modified to function as a nano-DESI source. Use of this existing platform enabled straightforward integration with the Waters mass spectrometer and imaging software. A photograph of the ion source is shown in *Figure S1, Supporting information*. The standard Prosolia transfer line was replaced by a prototype heated transfer line and sample cone assembly supplied by Waters (Waters Research Centre, Budapest), in order to promote desolvation of protein ions. The inlet temperature was set to 275 ^{o}C and allowed to equilibrate to allow for inlet expansion due to the temperature increase. This temperature matched the inlet temperature used for native nano-DESI on an orbitrap mass spectrometer previously.[1] The DESI sprayer assembly was replaced with a flame-pulled fused silica capillary (OD = 280 μm, ID = 75 μm as purchased then pulled to approx. 100 μm OD) connected to a syringe (10 mL, Hamilton, Reno, Nevada). The solvent system for native nano-DESI was 200 mM aqueous ammonium acetate at pH ~7 containing 0.125% C_8E_4 detergent by volume. Solvent flow was provided by the syringe and external syringe pump at a rate of 1.9 μL/min. A second flame-pulled capillary approx. 2 cm long was positioned at the exit of the first capillary, with an angle of approx. 50^{o} between the two. The second capillary was positioned approx. 0.5 mm within the center of the heated inlet without contacting the inlet sides. A microscope camera was used to aid capillary positioning and monitor the nano-DESI probe during analysis. The solvent was aspirated into the inlet by the mass spectrometer vacuum. A high voltage potential (1.8 kV) was applied to the solvent

through the syringe needle by a cable attached to the mass spectrometer high-voltage power supply.

NanoESI and LESA

NanoESI and LESA were performed with a Triversa NanoMate (Advion Biosciences, Ithaca, NY). Calibration of the time-of-flight (TOF) analyzer was performed by direct infusion nanoESI of sodium iodide solution. NanoESI of denatured ubiquitin, cytochrome C and apo-myoglobin in 50% MeOH + 0.1% formic acid was performed to calibrate the TWIMS device at three wave heights (24.5 V, 25.0 V and 25.5 V). $^{TW}CCS_{N2\rightarrow He}$ were calculated by a previously published method using a power function with R^2 >0.99.[2]

Native LESA was performed using 200 mM aqueous ammonium acetate with 0.125% C_8E_4 detergent for replicates at three wave heights (other mass spectrometer settings for LESA were as described for the nano-DESI imaging experiment, below). The 'contact' LESA method was used, where the pipette tip contacts the sample to contain the solvent. 5 μL of solvent was aspirated from the solvent well. Solvent was dispensed (1.9 μL) onto tissue, followed by a delay of 30s to allow diffusion of analytes into the solvent, then reaspiration of the solvent (2.2 μL). The sample was moved to the nanoESI chip and electrosprayed with a potential of 1.75 kV and backpressure of 0.15 PSI.

Ion mobility-mass spectrometry

The nano-DESI ion source or Triversa Nanomate was attached to a Synapt G2-S (Waters Corporation, Manchester, UK), a TWIMS-enabled orthogonal TOF mass spectrometer, and connected to the control computer using the commercial DESI electronics. The instrument and ion source were controlled through MassLynx (version 4.2, Waters) and were set to operate in 'Sensitivity' and 'positive ion' modes. A Speedivalve on the roughing pump was used to throttle the backing pressure to approx. 6 mBar to aid the transfer of protein ions from atmospheric pressure. It was important to set this pressure after the heated inlet reached operating temperature as the backing pressure decreased with increasing inlet temperature. The cone voltage was set to 80 V to remove detergent molecules and desolvate protein ions. Configuration of additional settings through the MassLynx MS Tune window was necessary for improved sensitivity and optimal TWIMS separation for protein ions. These settings include a manually defined quadrupole profile and TriWave settings, which are detailed in *Table S1, Supporting Information*. Vacuum chamber pressures after equilibration of manual gas settings at the start of the nano-DESI experiment) are found in *Table S2, Supporting information* and are representative of pressures used for all other TWIMS experiments in this article.

Nano-DESI imaging was performed with a travelling wave height of 25.0 V, with additional measurements of $^{TW}CCS_{N2\rightarrow He}$ performed at 24.5 V and 25.5 V; for LESA, three wave heights (24.5, 25.0, 25.5 V) were used.

For nano-DESI MSI, the experiment was defined in HDI (version 1.5, Waters) and leveraged the workflow of the commercial DESI source. A photograph of the microscope slide holding the tissue section was imported into HDI and the analysis region was defined. Basic acquisition parameters were specified in HDI and are included here in *Table S3, Supporting Information*. The experiment was exported to a .csv file and imported into MassLynx as a sample list. Data acquisition was triggered by starting the sample queue. Contact closure events initialized and synchronized the nano-DESI source and mass spectrometer during analysis. Imaging of the kidney took approx. 7 hours with a TOF scan time of 5 s, an X-axis rate of 20 μm/s and a Y-step of 300 μm. Masslynx, DriftScope (version 2.9, Waters) and ORIGAMI^{ANALYSE} (v1.2.1.4)[36] were used for data processing and visualization.

Ion image generation

The data file for the entire experiment was imported into DriftScope and manually interrogated for protein signals with reference to previous experiments that identified proteins by top-down MS.[1,3,29] A peak list featuring '*m/z*' in the first column and arrival time in the second column was constructed and saved as a tab-delimited text file. The text file was imported into HDI to specify peaks to process. The data were processed with a noise threshold of 1 count, *m/z* window of 0.5 and arrival time window of 5 bins to account for the protein peak width in each dimension. HDI then produced a new text file containing the processed data for visualization in the 'Analysis' tab. The data were normalized to total ion current. Ion images featuring multiple charge states of the same protein were produced using the "Add" function of the "Mass Composition" option in HDI post-normalization. Ion images had a nominal pixel size of 100 x 300 μm (0.03 mm^2) and had linear interpolation applied. The anatomy of the kidney is shown in *Figure S2*, *Supporting information*. The analyzed kidney section is shown in a bright-field image in *Figure S3a, Supporting Information*. The TIC ion image for the complete native nano-DESI experiment is shown in *Figure S3b, Supporting Information*, and the arrival time versus *m/z* plot is shown in *Figure S4, Supporting information*.

Trajectory model CCS_{He} calculations

Where the X-ray crystal structure was available for a protein, CCS_{He} was calculated by the trajectory method in IMoS (v. 1.10).[37] The default parameters for He gas were used.

Results and discussion

The effect of the heated inlet on CCS

To perform native nano-DESI mass spectrometry of proteins, it was beneficial to elevate the inlet temperature to improve desolvation and sensitivity. This requirement is the consequence of the need for relatively high solvent flow rates to maintain a stable solvent bridge during sampling. For comparison, the native nano-DESI flow rate is 1.9 µL/min whereas the nanoESI flow rate on the Triversa Nanomate is < 200 nL/min. In our previous native nano-DESI work using an orbitrap mass spectrometer, the inlet temperature was defined as 275 °C in the instrument software.[1] Here, a heated ion inlet was added to the TWIMS-enabled mass spectrometer for nano-DESI to improve desolvation of ions and sensitivity. Previous investigations of DESI MS for protein analysis have used a similar heated inlet for the same purpose.[15,38]

As described above, the integration of TWIMS into native nano-DESI MSI has the potential to improve the quality of ion images by allowing arrival time filtering, and to enable direct measurement of collision cross sections (CCSs) from tissue. An obvious question that arises is: do the elevated inlet temperatures associated with nano-DESI have the potential to disrupt protein structure?[38] To evaluate the effect, if any, of inlet temperature, the CCSs calculated following native nano-DESI of tissue were compared with those obtained following LESA, which does not require a heated inlet as it relies on nanoESI. Any significant protein unfolding due to inlet heating in nano-DESI should be detected as a greater $^{TW}CCS_{N2\rightarrow He}$ relative to that measured by LESA with an ambient temperature inlet.

A thin section of rat kidney was analyzed by nano-DESI with non-denaturing solvent using the TWIMS-MSI workflow. Specific locations within rat kidney (medulla, cortex) were also analyzed by native LESA-TWIMS MS using the same inlet but at ambient temperature. All other instrument conditions matched the native nano-DESI analysis. Native LESA $^{TW}CCS_{N2\rightarrow He}$ values were compared to $^{TW}CCS_{N2\rightarrow He}$ values obtained by native nano-DESI. The expected error in CCS determined in this manner is <5%.[7] Relatedly, we expect significant structure disruption due to inlet heating to be evident as nano-DESI $^{TW}CCS_{N2\rightarrow He}$ values >5% larger than LESA $^{TW}CCS_{N2\rightarrow He}$ values. A comparison of the nano-DESI $^{TW}CCS_{N2\rightarrow He}$ and the LESA $^{TW}CCS_{N2\rightarrow He}$ values are shown in **Table 1**.

The $^{TW}CCS_{N2\rightarrow He}$ for β-thymosin 4 (4^+, nano-DESI; 754 Å^2, LESA; 736 Å^2) and ubiquitin (5^+, nano-DESI; 1086 Å^2, LESA; 1083 Å^2) were similar to values obtained previously with LESA from mouse tissue (β-

thymosin; 733 Å^2, ubiquitin; 1047 Å^2).[2] (Note, amino acid sequences are identical in both organisms). The $^{TW}CCS_{N2\rightarrow He}$ for ubiquitin and cytochrome C are within the ranges of experimental values in the literature.[41] The CCS_{He} for the crystal structure of phosphatidylethanolamine binding protein (PEBP1, PDB: 2IQY) was calculated to be 1956 Å^2, approx. 10% larger than $^{TW}CCS_{N2\rightarrow He}$ for the 8^+ charge state determined by nano-DESI and LESA. Lower charge states of monomeric proteins can be expected to have smaller ^{TW}CCS than predicted from crystal structures.[42] The difference is suggestive of gas phase compaction of this protein due to the travelling wave height.[43,44]

The CCS_{He} (2980 Å^2) for the homotrimeric RidA protein assembly was determined *in silico* by calculation from the crystal structure coordinates (PDB: 1QAH). The calculated value compares to $^{TW}CCS_{N2\rightarrow He}$ obtained by nano-DESI for RidA charge states 10^+ (tentatively determined from the weak signals as 2865 Å^2, 4% smaller) and 11^+ (2788 Å^2, 6.9% smaller). With native LESA, the RidA $^{TW}CCS_{N2\rightarrow He}$ was measured to be 2785 Å^2 for the 11^+ charge state (10^+ not detected). The observation of gas phase compaction of protein assemblies is not unprecedented: We previously observed smaller experimental ^{TW}CCS (determined following LESA MS) relative to the CCS predicted from crystal structure coordinates of the hemoglobin heterotetramer and other reports have explored this phenomenon in depth.[4,42,43,45] Jurneczko and Barran measured the CCS of melittin (~2.9 kDa monomer) and hemoglobin (~64 kDa tetramer) to be 10% and 28% smaller for the lowest detected charge state than predicted from crystal structure coordinates, and generally noted increasing difference with increasing protein molecular weight. For the hemoglobin tetramer the difference was attributed to structural collapse owing to the volume of the central cavity.[42] Work by Hogan *et al.* using a differential mobility analyser suggested gas phase compaction of GroEL (~800 kDa tetradecamer) by as much as 40%.[46]

The data in **Table 1** indicate that measurable structure disruption did not occur for the investigated proteins due to the heated inlet used for nano-DESI. The $^{TW}CCS_{N2\rightarrow He}$ values obtained by LESA did not differ significantly from those obtained by nano-DESI.

***Table 1**: $^{TW}CCS_{N2\rightarrow He}$ for rat kidney proteins sampled by native nano-DESI and native LESA.*

Protein	Charge state	MW (kDa)	Nano-DESI $^{TW}CCS_{N2\rightarrow He}$ (Å^2)[a]	Nano-DESI Std Dev[b]	LESA $^{TW}CCS_{N2\rightarrow He}$ (Å^2)[a]	LESA Std Dev[b]	nano-DESI→LESA %difference
β-thymosin 4	3	5.0	652	6.8	679	4.4	-4.2
β-thymosin 4	4	5.0	754	9.0	736	13.8	2.4
Ubiquitin (-GG)	4	8.5	950	11.1	996	8.6	-4.9
Ubiquitin (-GG)	5	8.5	1092	6.3	1137	3.6	-4.1
Ubiquitin	4	8.6	951	14.1	1000	1.4	-5.1
Ubiquitin	5	8.6	1086	8.8	1083	23.7	0.3
Acyl-coA BP	5	9.9	1069	14.7	1075	3.5	-0.6
Cytochrome C	6	12.1	1266	21.1	1269	4.9	-0.3
Cytochrome C	6	12.1	1343	17.3	1378	3.1	-2.6
H-FABP	6	14.7	1372	33.8	1435	3.8	-4.6
H-FABP	7	14.7	1425	29.3	1464	1.4	-2.6
K-FABP	7	17.6	1525	23.4	1583	2.8	-3.8
MUP	7	18.7	1575	33.4	1630	12.1	-3.5
PEBP1	8	20.7	1760	43.9	1769	1.6	-0.5
RidA trimer	11	42.6	2788	66.4	2785	9.7	0.1

[a]*Mean of CCS values from three travelling wave heights (24.5 V, 25.0 V and 25.5 V)*
[b]*One standard deviation determined from CCS values obtained at three travelling wave heights.*

Arrival time filtering improves image specificity.

Arrival time (t_A) filtering can be used to subtract chemical noise from protein ion signals that overlap in *m/z* but differ by t_A.[15] We have previously used this strategy to produce native LESA MS images of proteins with reduced contribution by interfering signals, thus improving the contrast in the images.[4] **Figure 1** shows data associated with *m/z* 2676.2. This *m/z* corresponds to 7^+ charge state of major urinary protein (MUP). The arrival time distribution (ATD) for *m/z* 2676.2 (**Figure 1a**) shows two peaks marked by red and blue arrows. The mass spectrum without arrival time filtering is shown in **Figure 1b**.The mass spectra at the apex of each peak are shown in **Figure 1c** and **Figure 1d**. Only the spectrum shown in **Figure 1c** contains a peak corresponding to MUP^{7+}, with a calculated $^{TW}CCS_{N2\rightarrow He}$ of 1620 Å^2. The ion image produced using data from the entire ATD (**Figure 1e**) does not show any specific distribution. In contrast, the ion image produced using the filtered mass spectrum in **Figure 1f** shows the expected distribution of MUP, i.e., in the cortex tissue[47,48] (For anatomy, see *Figure S2, Supporting Information*). t_A filtering has a marked effect here because of the low intensity of the protein signals which are lost amongst the background in the unfiltered image. Signals attributable to chemical background and potentially unresolved protein ions with abundance in the medulla

tissue produce the image **Figure 1g** from the second peak in the ATD, which does not show the same distribution as **Figure 1f**.

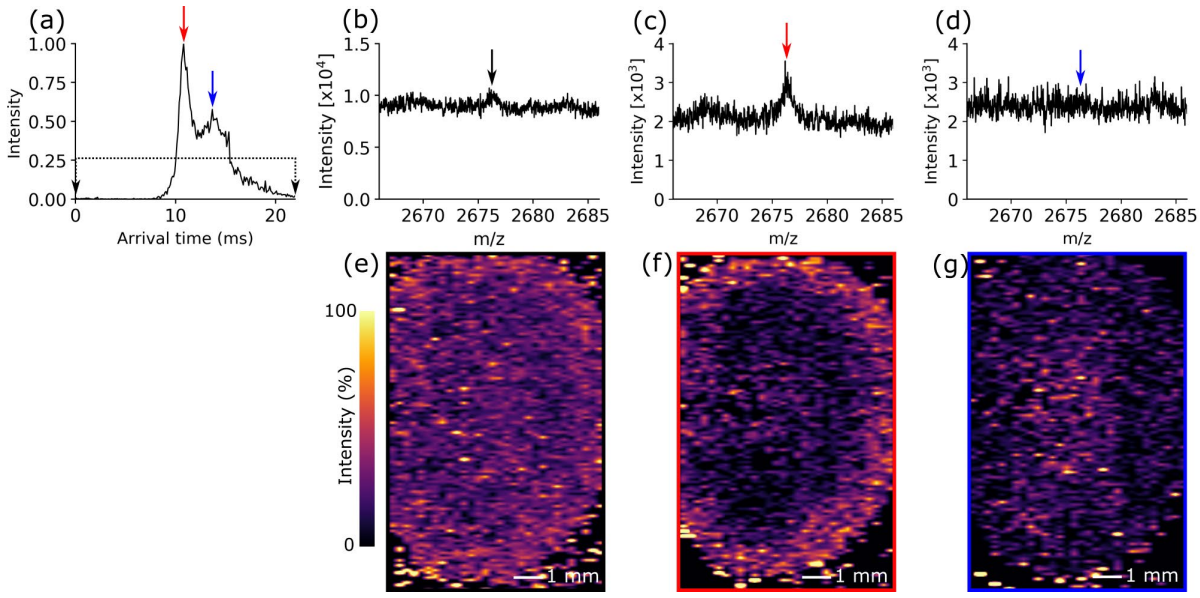

Figure 1: (a) The arrival time distribution for *m/z* 2676.2 acquired with a travelling wave height of 25 V. Red and blue arrows indicate two peak apexes. The total mass spectrum for all arrival times is shown in (b). The arrival time filtered mass spectrum at the red apex is shown in **(c)** and shows signals for major urinary protein 7^+ (MUP). The mass spectrum for the blue apex **(d)** does not show MUP signals. TIC normalized ion images were produced that include *m/z* signals for the full arrival time distribution (**(e)**, indicated by the black arrows in **(a)** and **(b)**), red apex **(f)** and blue apex **(g)**. Only the ion image **(f)** shows the distribution expected for MUP.

Figures S5-S9, Supporting Information further demonstrate ion images obtained through t_A-filtering of interfering signals for β-thymosin 4, cytochrome C, K-FABP, PEBP1, and H-FABP.

Analysis of proteins of MW <10 kDa

The results above show that t_A-filtering improves the specificity of protein ion images, and that it is possible to determine $^{TW}CCS_{N2\rightarrow He}$ values for endogenous proteins by nano-DESI TWIMS-MS. We subsequently produced t_A-filtered ion images incorporating multiple charge states of proteins from the kidney section. $^{TW}CCS_{N2\rightarrow He}$ (± 5%) at a travelling wave height of 25 V were calculated for each charge state of each protein. The total mass spectrum, total ion chronogram and total arrival time

distribution for the native nano-DESI-TWIMS MSI experiment are shown in *Figure S10*, *Supporting information*. The total arrival time versus *m/z* plot (*Figure S4*, *Supporting information*) shows the 2D separation of protein ions for the entire experiment.

Figure 2 shows ion images featuring two charge states of a range of abundant low molecular weight (< 10 kDa) proteins, together with arrival time-filtered mass spectra and ATDs. β-thymosin 4 (4.96 kDa, tentatively assigned here on the basis of intact mass and previously identified by top-down MS/MS[29]) is the smallest protein detected here and its ion image (**Figure 2a**) indicates its presence throughout the kidney tissue, but with a notably lower signal intensity in the cortex. The 4^+ charge state was determined to have a $^{TW}CCS_{N2\rightarrow He}$ of 759 °Å^2. There was a significant second peak in the ATD; however, the associated extracted mass spectrum did not contain peaks corresponding to β-thymosin 4 (See *Figure S5 Supporting Information*), so that ATD peak is not indicative of an unfolded conformer. The 3^+ charge state exhibited a smaller $^{TW}CCS_{N2\rightarrow He}$ (661 Å^2). The calculated $^{TW}CCS_{N2\rightarrow He}$ values for ubiquitin (8.65 kDa, tentatively assigned here on the basis of intact mass and previously identified by top-down MS/MS [29], **Figure 1b**) were 1094 Å^2 (5^+ charge state) and 971 Å^2 (4^+ charge state), in agreement with our previously reported values obtained by LESA MS^2 and the range of $^{DT}CCS_{He}$ values collated by *May et al*.[49]

The $^{TW}CCS_{N2\rightarrow He}$ values for ubiquitin lacking C-terminal diglycine (-GG, 8.45 kDa, **Figure 1c**) and acyl-coA binding protein (9.94 kDa, **Figure 1d**), both of which were tentatively assigned here on the basis of intact mass and identified previously by top-down MS/MS^2, have not been reported previously. Calculated $^{TW}CCS_{N2\rightarrow He}$ values for the truncated ubiquitin (5^+ charge state: 1101 Å^2; 4^+ charge state: 966 Å^2) were similar to those of ubiquitin, however, each protein exhibits a different spatial distribution. Ubiquitin signals were most intense in medullary tissue and in the renal pelvis, whilst ubiquitin (-GG) was most abundant in the cortex. This observation indicates different cell specificity and functionality. Acyl-coA binding protein (5^+ charge state: 1088 Å^2; 4^+ charge state: 1049 Å^2) was more homogenously distributed than other small proteins, with somewhat greater abundance in medulla and cortex tissues.

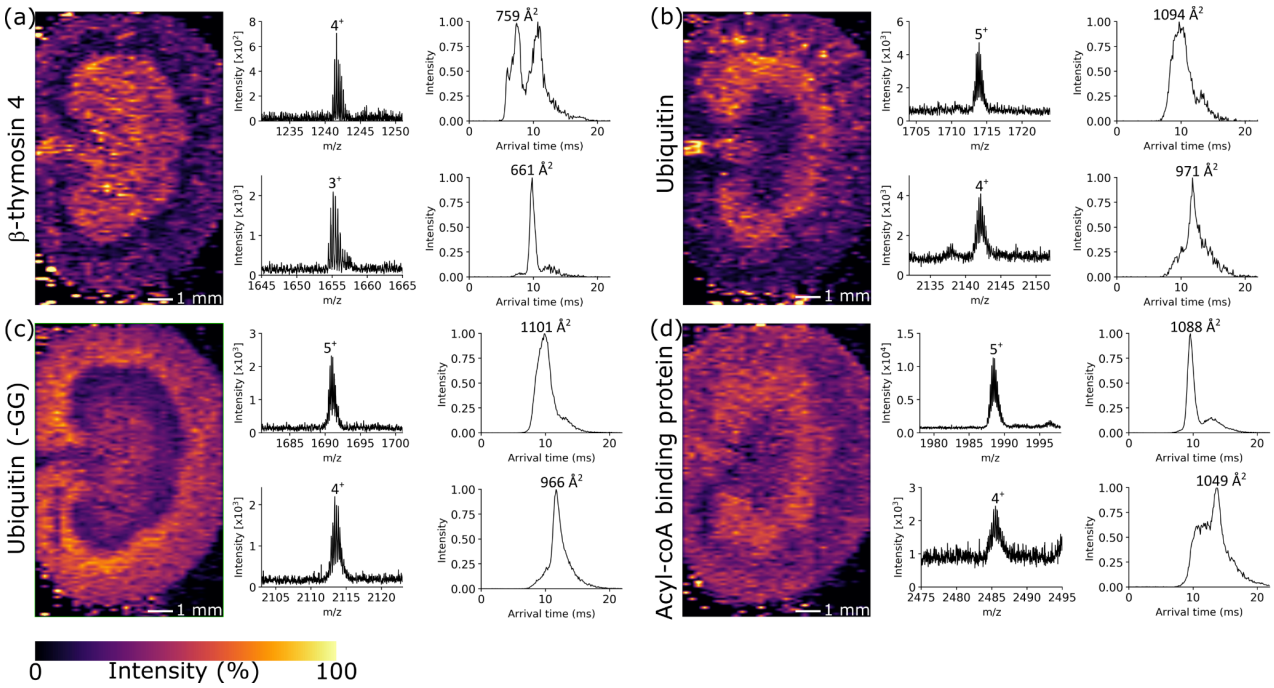

Figure 2: TIC normalized arrival time (t_A)-filtered ion images, t_A-filtered mass spectra and ATD plots for small proteins (MW<10 kDa) acquired with a travelling wave height of 25 V. Ion images are composites comprised of signals from the protein specific peak in each ATD and mass spectrum for two charge states of each protein; **(a)** β-thymosin 4, 4.96 kDa, abundant in central tissues and of low abundance in the cortex **(b)** ubiquitin, 8.65 kDa, abundant in medulla tissue **(c)** ubiquitin (-GG), 8.45 kDa, abundant in cortex tissue **(d)** acyl-coA binding protein, 9.94 kDa, comparatively homogenous distribution.

Proteins of MW > 10 kDa and protein complexes

Composite arrival time-filtered ion images, arrival time-filtered mass spectra and ATD plots are shown in **Figure 3** for proteins with MW ranging from 14.7 kDa – 42.6 kDa. The ion image in **Figure 3a** features the 7^+ ($^{TW}CCS_{N2\rightarrow He}$ 1466 A^2) and 6^+ ($^{TW}CCS_{N2\rightarrow He}$ 1419 A^2) charge states of heart-fatty acid-binding protein (H-FABP, tentatively assigned here on the basis of intact mass and identified previously by top-down MS/MS[3]). The observed spatial distribution is in good agreement with that observed previously by native LESA and native nano-DESI MSI, i.e., most abundant within the medulla tissue.[1,3] Kidney-fatty acid binding protein (K-FABP, tentatively assigned here on the basis of intact mass and previously identified by top-down MS/MS[3]) was most abundant in the cortex tissue (**Figure 3b**), and was detected as 7^+ ($^{TW}CCS_{N2\rightarrow He}$ 1558 Å^2) and 6^+ ($^{TW}CCS_{N2\rightarrow He}$ 1532 Å^2) ions. **Figure 3c** shows the composite ion image (8+ and 7+ charge states) for the homodimer of S100-A6 (tentatively assigned here on the basis of intact mass and identified previously by top-down MS/MS[1]). The dimer

is observed primarily in the renal pelvis in agreement with our previous work. [1] $^{TW}CCS_{N2\rightarrow He}$ values were determined for the two charge states; 8^+: 1791 Å^2 and 7^+: 1730 Å^2. The second peak in the ATD of the 8+ charge state corresponds to salt adducts of 4+ ions of acyl-coA binding protein. The S100-A6 dimer is not observed following sampling with LESA and so comparison between techniques is not currently possible. The intact homotrimer Reactive intermediate deiminase A (RidA, tentatively assigned here on the basis of intact mass and identified previously by top-down MS[3] [3]) was observed in the cortex (**Figure 3d**). The signal is limited for this protein, in part because of the gentle ionization conditions which limit the desolvation of larger proteins on QTOF mass spectrometers.[50] Nevertheless, evidence from two previous native MSI studies[1,3] and immunohistology[51,52] correlates with the distribution observed here. Both the 11^+ ($^{TW}CCS_{N2\rightarrow He}$ 2881 Å^2) and 10^+ ($^{TW}CCS_{N2\rightarrow He}$ 2865 Å^2) charge states were observed.

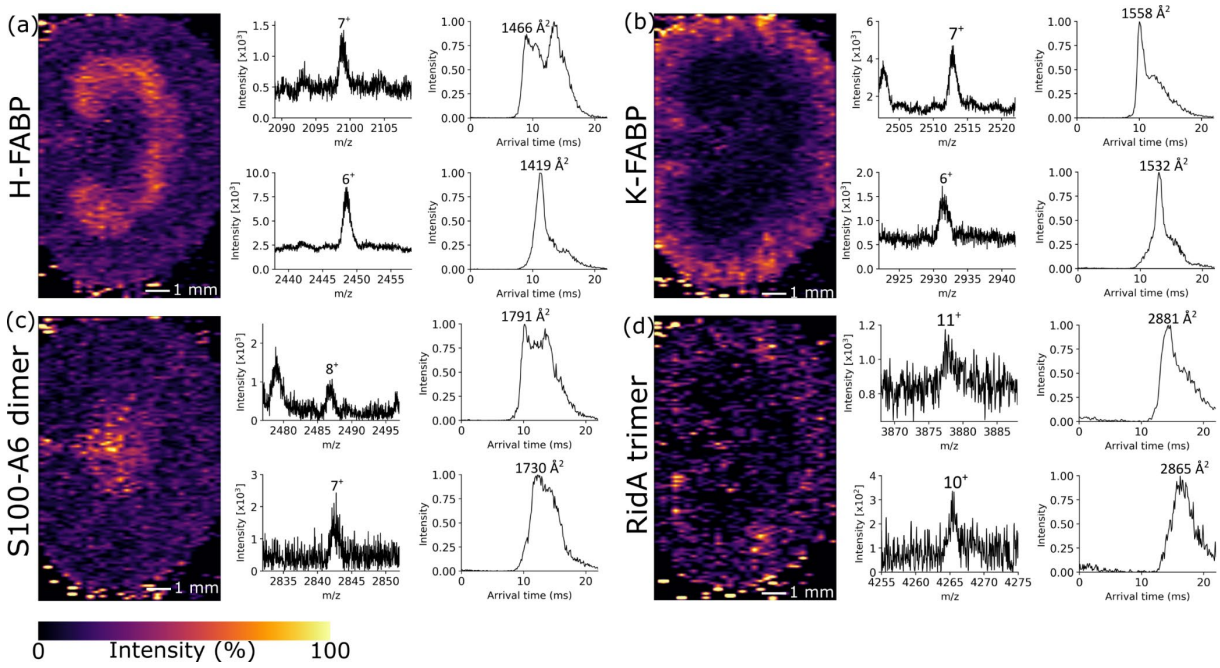

Figure 3: TIC normalized t_A-filtered ion images, t_A-filtered mass spectra and ATD plots for proteins from 14.7 kDa – 42.6 kDa acquired with a travelling wave height of 25 V. Ion images are composites comprised of signals from the protein specific peak in each ATD and mass spectrum for two charge states of each protein. (a) H-FABP, 14.7 kDa, most abundant in the medulla. (b) K-FABP, 17.6 kDa, most abundant in the cortex. (c) S100-A6 homodimer, 19.9 kDa, abundant in the renal pelvis. (d) RidA homotrimer, 42.6 kDa, most abundant in the cortex tissue.

Conclusions

The results show that native nano-DESI MSI featuring ion mobility separation is a viable technique for improving ion image specificity for native MSI. Simultaneously, it enables investigation of the tissue specificity of folded protein conformers using both *m/z* and CCS.

$^{TW}CCS_{N2\rightarrow He}$ obtained from independent native nano-DESI and native LESA experiments showed no deviance outside of expected error for TWIMS, indicating that native nano-DESI with supplemental heating is suitably soft for structural interrogation of endogenous proteins and protein complexes. Experimental $^{TW}CCS_{N2\rightarrow He}$ values were in good agreement with literature values and CCSs calculated for x-ray crystal structures where available.

Incorporation of TWIMS into native nano-DESI MSI reduced the contribution of non-specific signals to ion images, thereby improving their quality. Potentially, native nano-DESI could be coupled to other ion mobility techniques (i.e. other than TWIMS) to benefit from similar background signal reduction. State of the art higher resolution IMS, e.g., cyclicTWIMS[53] and TIMS[54], could further resolve overlapping protein signals, reduce background signal and provide CCS. Where these devices are available commercially, they are coupled to state-of-the-art mass spectrometers which could provide higher sensitivity under the gentle conditions required to preserve folded structures. Native MS-compatible differential ion mobility separators could also be used to reduce background signals, but do not currently enable CCS to be determined.[34] Future efforts must focus on increasing the variety of detectable proteins, e.g., through enhanced sample preparation, to increase the applicability of native nano-DESI-TWIMS MSI to structural biology research.

Acknowledgments

HJC is an EPSRC Established Career Fellow (EP/S002979/1). OJH is funded by EPSRC (EP/S002979/1). The Waters DESI source was funded by EPSRC (EP/S002979/1). The Triversa NanoMate and Synapt G2-S mass spectrometer were funded by EPSRC (EP/K039245/1). The authors thank Mike Morris and Tamas Karancsi of Waters for supply of the prototype heated transfer line and sample cone assembly. Supplementary data supporting this research is openly available from the University of Birmingham data archive at DOI: *to be supplied on acceptance*.

ORCID IDs

HJC: 0000-0003-4590-9384

OJH: 0000-0002-2286-5780

References

(1) Hale, O. J.; Cooper, H. J. Native Mass Spectrometry Imaging of Proteins and Protein Complexes by Nano-DESI *Anal Chem* **2021**, *93*, 4619-4627.
(2) Griffiths, R. L.; Sisley, E. K.; Lopez-Clavijo, A. F.; Simmonds, A. L.; Styles, I. B.; Cooper, H. J. Native mass spectrometry imaging of intact proteins and protein complexes in thin tissue sections *Int J Mass Spectrom* **2019**, *437*, 23-29.
(3) Hale, O. J.; Cooper, H. J. Native Mass Spectrometry Imaging and In Situ Top-Down Identification of Intact Proteins Directly from Tissue *J Am Soc Mass Spectrom* **2020**, *31*, 2531-2537.
(4) Hale, O. J.; Sisley, E. K.; Griffiths, R. L.; Styles, I. B.; Cooper, H. J. Native LESA TWIMS-MSI: Spatial, Conformational, and Mass Analysis of Proteins and Protein Complexes *J Am Soc Mass Spectrom* **2020**, *31*, 873-879.
(5) Marcoux, J.; Robinson, C. V. Twenty years of gas phase structural biology *Structure* **2013**, *21*, 1541-1550.
(6) Ruotolo, B. T.; Benesch, J. L.; Sandercock, A. M.; Hyung, S. J.; Robinson, C. V. Ion mobility-mass spectrometry analysis of large protein complexes *Nat Protoc* **2008**, *3*, 1139-1152.
(7) Bush, M. F.; Hall, Z.; Giles, K.; Hoyes, J.; Robinson, C. V.; Ruotolo, B. T. Collision cross sections of proteins and their complexes: a calibration framework and database for gas-phase structural biology *Anal Chem* **2010**, *82*, 9557-9565.
(8) Michaelevski, I.; Kirshenbaum, N.; Sharon, M. T-wave ion mobility-mass spectrometry: basic experimental procedures for protein complex analysis *J Vis Exp* **2010**.
(9) DeToma, A. S.; Salamekh, S.; Ramamoorthy, A.; Lim, M. H. Misfolded proteins in Alzheimer's disease and type II diabetes *Chem Soc Rev* **2012**, *41*, 608-621.
(10) Cybulsky, A. V. Endoplasmic reticulum stress, the unfolded protein response and autophagy in kidney diseases *Nat Rev Nephrol* **2017**, *13*, 681-696.
(11) Jaunmuktane, Z.; Brandner, S. Transmissible human proteopathies: an expanding field *Diagnostic Histopathology* **2019**, *25*, 16-22.
(12) Takats, Z.; Wiseman, J. M.; Gologan, B.; Cooks, R. G. Mass spectrometry sampling under ambient conditions with desorption electrospray ionization *Science* **2004**, *306*, 471-473.
(13) Kertesz, V.; Van Berkel, G. J. Fully automated liquid extraction-based surface sampling and ionization using a chip-based robotic nanoelectrospray platform *J Mass Spectrom* **2010**, *45*, 252-260.
(14) Roach, P. J.; Laskin, J.; Laskin, A. Nanospray desorption electrospray ionization: an ambient method for liquid-extraction surface sampling in mass spectrometry *Analyst* **2010**, *135*, 2233-2236.
(15) Towers, M. W.; Karancsi, T.; Jones, E. A.; Pringle, S. D.; Claude, E. Optimised Desorption Electrospray Ionisation Mass Spectrometry Imaging (DESI-MSI) for the Analysis of Proteins/Peptides Directly from Tissue Sections on a Travelling Wave Ion Mobility Q-ToF *J Am Soc Mass Spectrom* **2018**, *29*, 2456-2466.
(16) Garza, K. Y.; Feider, C. L.; Klein, D. R.; Rosenberg, J. A.; Brodbelt, J. S.; Eberlin, L. S. Desorption Electrospray Ionization Mass Spectrometry Imaging of Proteins Directly from Biological Tissue Sections *Anal Chem* **2018**, *90*, 7785-7789.
(17) Laskin, J.; Heath, B. S.; Roach, P. J.; Cazares, L.; Semmes, O. J. Tissue imaging using nanospray desorption electrospray ionization mass spectrometry *Anal Chem* **2012**, *84*, 141-148.
(18) Yin, R.; Kyle, J.; Burnum-Johnson, K.; Bloodsworth, K. J.; Sussel, L.; Ansong, C.; Laskin, J. High Spatial Resolution Imaging of Mouse Pancreatic Islets Using Nanospray Desorption Electrospray Ionization Mass Spectrometry *Anal Chem* **2018**, *90*, 6548-6555.
(19) Hsu, C. C.; Chou, P. T.; Zare, R. N. Imaging of Proteins in Tissue Samples Using Nanospray Desorption Electrospray Ionization Mass Spectrometry *Anal Chem* **2015**, *87*, 11171-11175.
(20) Lin, L. E.; Chen, C. L.; Huang, Y. C.; Chung, H. H.; Lin, C. W.; Chen, K. C.; Peng, Y. J.; Ding, S. T.; Wang, M. Y.; Shen, T. L.; Hsu, C. C. Precision biomarker discovery powered by microscopy image fusion-assisted high spatial resolution ambient ionization mass spectrometry imaging *Anal Chim Acta* **2020**, *1100*, 75-87.

(21) Kiss, A.; Smith, D. F.; Reschke, B. R.; Powell, M. J.; Heeren, R. M. Top-down mass spectrometry imaging of intact proteins by laser ablation ESI FT-ICR MS *Proteomics* **2014**, *14*, 1283-1289.
(22) Kooijman, P. C.; Mathew, A.; Ellis, S. R.; Heeren, R. M. A. Infrared Laser Desorption and Electrospray Ionisation of Non-Covalent Protein Complexes: Generation of Intact, Multiply Charged Species *Analysis & Sensing* **2021**, *1*, 44-47.
(23) Ekelöf, M.; Dodds, J.; Khodjaniyazova, S.; Garrard, K. P.; Baker, E. S.; Muddiman, D. C. Coupling IR-MALDESI with Drift Tube Ion Mobility-Mass Spectrometry for High-Throughput Screening and Imaging Applications *J Am Soc Mass Spectrom* **2020**, *31*, 642-650.
(24) Ryan, D. J.; Patterson, N. H.; Putnam, N. E.; Wilde, A. D.; Weiss, A.; Perry, W. J.; Cassat, J. E.; Skaar, E. P.; Caprioli, R. M.; Spraggins, J. M. MicroLESA: Integrating Autofluorescence Microscopy, In Situ Micro-Digestions, and Liquid Extraction Surface Analysis for High Spatial Resolution Targeted Proteomic Studies *Anal Chem* **2019**, *91*, 7578-7585.
(25) Piehowski, P. D.; Zhu, Y.; Bramer, L. M.; Stratton, K. G.; Zhao, R.; Orton, D. J.; Moore, R. J.; Yuan, J.; Mitchell, H. D.; Gao, Y.; Webb-Robertson, B.-J. M.; Dey, S. K.; Kelly, R. T.; Burnum-Johnson, K. E. Automated mass spectrometry imaging of over 2000 proteins from tissue sections at 100-µm spatial resolution *Nat Commun* **2020**, *11*, 8.
(26) Otsuka, Y.; Kamihoriuchi, B.; Takeuchi, A.; Iwata, F.; Tortorella, S.; Matsumoto, T. High-Spatial-Resolution Multimodal Imaging by Tapping-Mode Scanning Probe Electrospray Ionization with Feedback Control *Anal Chem* **2021**, *93*, 2263-2272.
(27) Lee, J. K.; Jansson, E. T.; Nam, H. G.; Zare, R. N. High-Resolution Live-Cell Imaging and Analysis by Laser Desorption/Ionization Droplet Delivery Mass Spectrometry *Anal Chem* **2016**, *88*, 5453-5461.
(28) Gan, J.; Ben-Nissan, G.; Arkind, G.; Tarnavsky, M.; Trudeau, D.; Noda Garcia, L.; Tawfik, D. S.; Sharon, M. Native Mass Spectrometry of Recombinant Proteins from Crude Cell Lysates *Anal Chem* **2017**, *89*, 4398-4404.
(29) Griffiths, R. L.; Creese, A. J.; Race, A. M.; Bunch, J.; Cooper, H. J. LESA FAIMS Mass Spectrometry for the Spatial Profiling of Proteins from Tissue *Anal Chem* **2016**, *88*, 6758-6766.
(30) Griffiths, R. L.; Hughes, J. W.; Abbatiello, S. E.; Belford, M. W.; Styles, I. B.; Cooper, H. J. Comprehensive LESA Mass Spectrometry Imaging of Intact Proteins by Integration of Cylindrical FAIMS *Anal Chem* **2020**, *92*, 2885-2890.
(31) Feider, C. L.; Elizondo, N.; Eberlin, L. S. Ambient Ionization and FAIMS Mass Spectrometry for Enhanced Imaging of Multiply Charged Molecular Ions in Biological Tissues *Anal Chem* **2016**, *88*, 11533-11541.
(32) Giles, K.; Pringle, S. D.; Worthington, K. R.; Little, D.; Wildgoose, J. L.; Bateman, R. H. Applications of a travelling wave-based radio-frequency-only stacked ring ion guide *Rapid Commun Mass Spectrom* **2004**, *18*, 2401-2414.
(33) Guevremont, R. High-field asymmetric waveform ion mobility spectrometry: a new tool for mass spectrometry *J Chromatogr A* **2004**, *1058*, 3-19.
(34) Hale, O. J.; Illes-Toth, E.; Mize, T. H.; Cooper, H. J. High-Field Asymmetric Waveform Ion Mobility Spectrometry and Native Mass Spectrometry: Analysis of Intact Protein Assemblies and Protein Complexes *Anal Chem* **2020**, *92*, 6811-6816.
(35) Mesa Sanchez, D.; Creger, S.; Singla, V.; Kurulugama, R. T.; Fjeldsted, J.; Laskin, J. Ion Mobility-Mass Spectrometry Imaging Workflow *J Am Soc Mass Spectrom* **2020**, *31*, 2437-2442.
(36) Migas, L. G.; France, A. P.; Bellina, B.; Barran, P. E. ORIGAMI: A software suite for activated ion mobility mass spectrometry (aIM-MS) applied to multimeric protein assemblies *Int J Mass Spectrom* **2018**, *427*, 20-28.
(37) Larriba-Andaluz, C.; Hogan, C. J., Jr. Collision cross section calculations for polyatomic ions considering rotating diatomic/linear gas molecules *J Chem Phys* **2014**, *141*, 194107.
(38) Yan, B.; Bunch, J. Probing Folded Proteins and Intact Protein Complexes by Desorption Electrospray Ionization Mass Spectrometry *J Am Soc Mass Spectrom* **2021**, *32*, 690-699.
(39) Wojcik, R.; Nagy, G.; Attah, I. K.; Webb, I. K.; Garimella, S. V. B.; Weitz, K. K.; Hollerbach, A.; Monroe, M. E.; Ligare, M. R.; Nielson, F. F.; Norheim, R. V.; Renslow, R. S.; Metz, T. O.; Ibrahim, Y. M.;

Smith, R. D. SLIM Ultrahigh Resolution Ion Mobility Spectrometry Separations of Isotopologues and Isotopomers Reveal Mobility Shifts due to Mass Distribution Changes *Anal Chem* **2019**, *91*, 11952-11962.
(40) Hollerbach, A. L.; Conant, C. R.; Nagy, G.; Monroe, M. E.; Gupta, K.; Donor, M.; Giberson, C. M.; Garimella, S. V. B.; Smith, R. D.; Ibrahim, Y. M. Dynamic Time-Warping Correction for Shifts in Ultrahigh Resolving Power Ion Mobility Spectrometry and Structures for Lossless Ion Manipulations *J Am Soc Mass Spectrom* **2021**.
(41) May, J. C.; McLean, J. A. Ion mobility-mass spectrometry: time-dispersive instrumentation *Anal Chem* **2015**, *87*, 1422-1436.
(42) Jurneczko, E.; Barran, P. E. How useful is ion mobility mass spectrometry for structural biology? The relationship between protein crystal structures and their collision cross sections in the gas phase *Analyst* **2011**, *136*, 20-28.
(43) Michaelevski, I.; Eisenstein, M.; Sharon, M. Gas-phase compaction and unfolding of protein structures *Anal Chem* **2010**, *82*, 9484-9491.
(44) Devine, P. W. A.; Fisher, H. C.; Calabrese, A. N.; Whelan, F.; Higazi, D. R.; Potts, J. R.; Lowe, D. C.; Radford, S. E.; Ashcroft, A. E. Investigating the Structural Compaction of Biomolecules Upon Transition to the Gas-Phase Using ESI-TWIMS-MS *J Am Soc Mass Spectrom* **2017**, *28*, 1855-1862.
(45) Hoaglund-Hyzer, C. S.; Counterman, A. E.; Clemmer, D. E. Anhydrous protein ions *Chem Rev* **1999**, *99*, 3037-3080.
(46) Hogan, C. J.; Ruotolo, B. T.; Robinson, C. V.; Fernandez de la Mora, J. Tandem Differential Mobility Analysis-Mass Spectrometry Reveals Partial Gas-Phase Collapse of the GroEL Complex *The Journal of Physical Chemistry B* **2011**, *115*, 3614-3621.
(47) Burnett, V. L.; Short, B. G.; Swenberg, J. A. Localization of alpha 2u-globulin within protein droplets of male rat kidney: immunohistochemistry using perfusion-fixed, GMA-embedded tissue sections *J Histochem Cytochem* **1989**, *37*, 813-818.
(48) Gomez-Baena, G.; Armstrong, S. D.; Phelan, M. M.; Hurst, J. L.; Beynon, R. J. The major urinary protein system in the rat *Biochem Soc Trans* **2014**, *42*, 886-892.
(49) May, J. C.; Jurneczko, E.; Stow, S. M.; Kratochvil, I.; Kalkhof, S.; McLean, J. A. Conformational Landscapes of Ubiquitin, Cytochrome c, and Myoglobin: Uniform Field Ion Mobility Measurements in Helium and Nitrogen Drift Gas *Int J Mass Spectrom* **2018**, *427*, 79-90.
(50) Snijder, J.; Rose, R. J.; Veesler, D.; Johnson, J. E.; Heck, A. J. Studying 18 MDa virus assemblies with native mass spectrometry *Angew Chem Int Ed Engl* **2013**, *52*, 4020-4023.
(51) Oka, T.; Tsuji, H.; Noda, C.; Sakai, K.; Hong, Y. M.; Suzuki, I.; Munoz, S.; Natori, Y. Isolation and characterization of a novel perchloric acid-soluble protein inhibiting cell-free protein synthesis *J Biol Chem* **1995**, *270*, 30060-30067.
(52) Schmiedeknecht, G.; Kerkhoff, C.; Orso, E.; Stohr, J.; Aslanidis, C.; Nagy, G. M.; Knuechel, R.; Schmitz, G. Isolation and characterization of a 14.5-kDa trichloroacetic-acid-soluble translational inhibitor protein from human monocytes that is upregulated upon cellular differentiation *Eur J Biochem* **1996**, *242*, 339-351.
(53) Giles, K.; Ujma, J.; Wildgoose, J.; Pringle, S.; Richardson, K.; Langridge, D.; Green, M. A Cyclic Ion Mobility-Mass Spectrometry System *Anal Chem* **2019**, *91*, 8564-8573.
(54) Fernandez-Lima, F.; Kaplan, D. A.; Suetering, J.; Park, M. A. Gas-phase separation using a trapped ion mobility spectrometer *Int J Ion Mobil Spectrom* **2011**, *14*.

TOC graphic

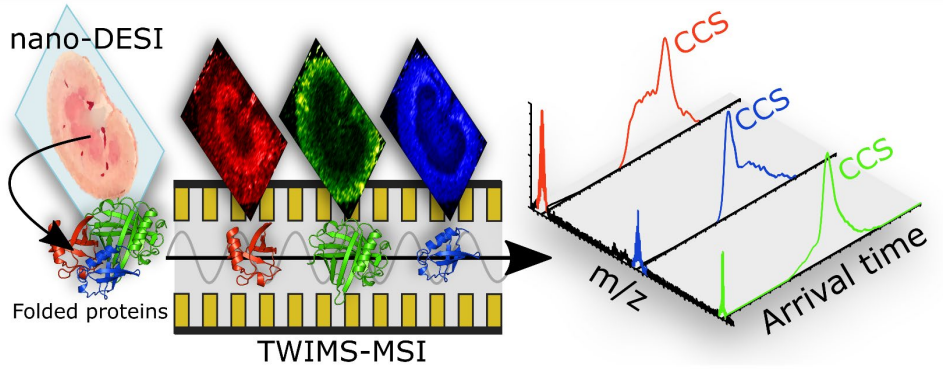
nano-DESI
Folded proteins
TWIMS-MSI
CCS
CCS
CCS
m/z
Arrival time